Impacts of Distributed PV in a Smart Grid using Temperature-Dependent Power Flow

Arif Ahmed*, Fiona Stevens McFadden† and Ramesh Rayudu‡
*†Robinson Research Institute
*‡Smart Power and Renewable Energy Systems Group
*†‡School of Engineering and Computer Science
Victoria University of Wellington
Wellington 6140, New Zealand
Email: *arif.ahmed@vuw.ac.nz, †fiona.stevensmcfadden@vuw.ac.nz and ‡ramesh.rayudu@vuw.ac.nz

***Abstract*—Power flow (PF) is the foundation of many power system analyses essential for power system studies. The evolution of modern smart networks with increasing levels of integrated Distributed Generation, communication infrastructure, automation and control, requires accurate power flow analysis. The conventional PF assumes the power network and equipment has constant impedances despite resistance being a strong function of temperature. This means that the subsequent analyses undertaken have an inherent temperature dependent error. This error could be reduced by using the Temperature-Dependent Power Flow (TDPF) algorithm which estimates the network branch temperatures and adjusts the network impedances and outputs the PF. In this paper, the TDPF is derived in rectangular form and utilised to investigate the network voltage, branch power loss, and branch temperatures with integrated distributed photovoltaic systems. Simulation performed on the IEEE 14-bus network shows convincing results and the benefit of using the TDPF technique.**

***Index Terms*—Impact study of distributed generation, Photovoltaic systems, Power flow algorithm, Temperature-dependent power flow, PV Integration**

I. Introduction

Power networks have evolved into smart grids [1] having capabilities of bi-directional power flows, distributed generation integration, communication infrastructure, demand response etc. Significant work is currently being undertaken to constantly make the grid smarter. Integration of distributed generation like the Photovoltaic (PV) system injects power in the opposite direction to conventional grid PF. This introduces and amplifies a number of problems in the network that includes voltage rise, reverse power flow, voltage instability, network power loss, etc. [2]–[4]. To accurately analyse these effects on the smart grid, accurate power flow analysis techniques are required.

The power flow is fundamental to a number of power system analyses, such as planning and design, stability studies, contingency studies, and security analysis [3], [5], [6]. A power flow problem involves solving nonlinear functions to calculate important power system states that represent the power system network [3], [5], [6]. The most common method to solve a power flow problem is the Newton-Raphson method due to its simplicity in implementation and faster convergence. The conventional PF is a good tool, but not the best tool as it has an inherent error due to the lack of temperature dependence in its formulation [7]. The resistance of a conductor is a strong function of temperature and it is an important characteristic to be considered in the power flow problem [7], [8]. The absence of a temperature effect in the conventional PF can yield significant errors in the power loss and power flow estimates under heavily loaded conditions (up to 30% for individual branches) [7], [9]. This will cause subsequent power system analyses to be erroneous which are essential to power system operators. The improved estimates calculated from a PF analysis with the temperature dependencies accounted for will improve the accuracy of these subsequent analyses and give improved information to the operators. Moreover, the impacts of PV integration needs to be assessed in an accurate setting i.e. considering temperature-dependent characteristics of the network.

This study, therefore, examines the impacts of distributed PV integrated in a power network using the more accurate Temperature-Dependent Power Flow (TDPF) [7] algorithm. The algorithm takes into account the resistance-temperature relationship of conductors and integrates it into the conventional PF technique. Moreover, the TDPF can be utilized to estimate the temperature of the conductors as well which is beneficial to Dynamic Thermal Line Rating (DTLR) [10], [11].

In this manuscript, the TDPF is derived in rectangular form for the study due to its simplicity in coding and implementation in MATLAB. This manuscript makes a contribution by deriving the TDPF algorithm in rectangular form capable of steady-state time-series power flow analysis. It also integrates distributed PV systems in the power flow algorithm and finally quantifies the impacts of distributed PV integration by calculating the temperature profiles, power loss profiles, and voltage profiles via simulation of the IEEE 14-Bus network using TDPF.

Section II of the manuscript presents the derivation of the TDPF in rectangular form, Section III discusses the solar PV modeling and data used in the study followed by Section IV which presents the modified IEEE 14-Bus network. Simulation results are discussed in Section V and the manuscript is concluded in Section VI.

978-1-5386-4950-3/17/$31.00 ©2017 IEEE

II. Derivation of the Temperature-Dependent Power Flow

The resistance of metallic conductors can be related to the temperature [8], [9] by

$$R(T_c) = R(T_{\text{Ref}})[1 + \alpha(T_c - T_{\text{Ref}})] \tag{1}$$

where, $R(T_c)$ is the conductor resistance at conductor temperature, T_c, $R(T_{\text{Ref}})$ is the conductor resistance at conductor reference temperature, T_{Ref}, and α is the temperature coefficient of resistance at T_{Ref}. The well-known thermal resistance model sufficiently models power system equipment [7]. The thermal resistance model assumes a linear relationship between device temperature rise and heat flow or losses out of the device. The thermal resistance [7] can be defined as

$$R_\theta = \frac{T_{\text{Rise}}}{P_{\text{Loss}}} = \frac{T_{\text{RatedRise}}}{P_{\text{RatedLoss}}} \tag{2}$$

In Equation (2), T_{Rise} is the difference between the conductor temperature and the ambient temperature. Hence, Equation (2) can be written as

$$T_c = T_{\text{ambient}} + R_\theta P_{\text{Loss}} \tag{3}$$

For any conductor, given the thermal resistance, R_θ, the temperature can be calculated using Equation (3). The power loss, $P_{\text{Loss,ij}}$, between Bus-i and Bus-j for a two bus network can be calculated as

$$\begin{aligned} P_{\text{Loss},ij} = \text{Re}\{&(V_{r_i} + jV_{m_i})(I_{r_{ij}} + jI_{m_{ij}})^* \\ &+ (V_{r_j} + jV_{m_j})(I_{r_{ji}} + jI_{m_{ji}})^*\} \end{aligned} \tag{4}$$

V_r is the real part of the complex voltage and V_m is the imaginary part of the complex voltage. Similarly, I_r is the real part of the complex current and I_m is the imaginary part of the complex current. Simplification of Equation (4) results in Equation (5).

$$\begin{aligned} P_{\text{Loss},ij} = (&V_{r_i}^2 + V_{r_j}^2 + V_{m_i}^2 + V_{m_j}^2 \\ &- 2V_{r_i}V_{r_j} - 2V_{m_i}V_{m_j})g_{ij} \end{aligned} \tag{5}$$

g_{ij} is the conductance of the branch between Bus-i and Bus-j. From Equation (5), for any branch conductor, the conductor temperature can be calculated by substitution of Equation (5) in Equation (3), which yields

$$\begin{aligned} T_c = T_{\text{ambient}} + &R_{\theta,ij}(V_{r_i}^2 + V_{r_j}^2 + V_{m_i}^2 \\ &+ V_{m_j}^2 - 2V_{r_i}V_{r_j} - 2V_{m_i}V_{m_j})g_{ij} \end{aligned} \tag{6}$$

Equation (6) is essential to deriving the TDPF algorithm. An implicit temperature difference equation [7] can be defined based on Equation (6) for any branch between Bus-i and Bus-j, which will be integrated into the conventional PF to derive the TDPF algorithm. The implicit temperature difference equation is defined as

$$H_{ij} = T_{ij} - (T_{\text{ambient}} + R_{\theta,ij}P_{\text{Loss},ij}) = 0 \tag{7}$$

The temperature difference mismatch equation is therefore

$$\Delta H_{ij} = 0 - [T_{ij} - (T_{\text{ambient}} + R_{\theta,ij}P_{\text{Loss},ij})] \tag{8}$$

The temperature difference mismatch vector is appended to the conventional PF [3], [5], [12] to derive the update equation of the TDPF as

$$\begin{bmatrix} \boldsymbol{V_r} \\ \boldsymbol{V_m} \\ \boldsymbol{T} \end{bmatrix}^{(v+1)} = \begin{bmatrix} \boldsymbol{V_r} \\ \boldsymbol{V_m} \\ \boldsymbol{T} \end{bmatrix}^{(v)} + \boldsymbol{J}^{-1(v)} \begin{bmatrix} \boldsymbol{\Delta P} \\ \boldsymbol{\Delta Q} \\ \boldsymbol{\Delta V^2} \\ \boldsymbol{\Delta H} \end{bmatrix}^{(v)} \tag{9}$$

In Equation (9), v is the iteration number, $\boldsymbol{V_r}$ is the vector of real voltages, $\boldsymbol{V_m}$ is the vector of imaginary voltages, $\boldsymbol{T}$ is the vector of branch temperatures, $\boldsymbol{\Delta P}$ is the vector of real power mismatch, $\boldsymbol{\Delta Q}$ is the vector of reactive power mismatch, $\boldsymbol{\Delta V^2}$ is the vector of the square of the voltage magnitude, and $\boldsymbol{\Delta H}$ is the temperature difference mismatch vector. The additional elements in the Jacobian, $\boldsymbol{J}$, in Equation (9) which are not included in the conventional PF are given by Equations (11), (12), (13) (14), (15), and (16).

$$\boldsymbol{J}_{new} = \begin{bmatrix} \frac{\partial \boldsymbol{P}}{\partial \boldsymbol{V_r}} & \frac{\partial \boldsymbol{P}}{\partial \boldsymbol{V_m}} & \frac{\partial \boldsymbol{P}}{\partial \boldsymbol{T}} \\ \frac{\partial \boldsymbol{Q}}{\partial \boldsymbol{V_r}} & \frac{\partial \boldsymbol{Q}}{\partial \boldsymbol{V_m}} & \frac{\partial \boldsymbol{Q}}{\partial \boldsymbol{T}} \\ \frac{\partial \boldsymbol{V^2}}{\partial \boldsymbol{V_r}} & \frac{\partial \boldsymbol{V^2}}{\partial \boldsymbol{V_m}} & \frac{\partial \boldsymbol{V^2}}{\partial \boldsymbol{T}} \\ \frac{\partial \boldsymbol{H}}{\partial \boldsymbol{V_r}} & \frac{\partial \boldsymbol{H}}{\partial \boldsymbol{V_m}} & \frac{\partial \boldsymbol{H}}{\partial \boldsymbol{T}} \end{bmatrix} \tag{10}$$

The partial derivatives of the new elements of the Jacobian in Equation (13) are

$$\frac{\partial V_k^2}{\partial T_{ij}} = 0 \text{ for any } i, j \tag{14}$$

$$\frac{\partial H_{ij}}{\partial V_{r_k}} = \begin{cases} -2R_\theta(V_{r_i} - V_{r_j})g_{ij} & \text{for } k = i \\ -2R_\theta(V_{r_j} - V_{r_i})g_{ij} & \text{for } k = j \\ 0 & \text{for } k \neq i, k \end{cases} \tag{15}$$

$$\frac{\partial H_{ij}}{\partial V_{m_k}} = \begin{cases} -2R_\theta(V_{m_i} - V_{m_j})g_{ij} & \text{for } k = i \\ -2R_\theta(V_{m_j} - V_{m_i})g_{ij} & \text{for } k = j \\ 0 & \text{for } k \neq i, k \end{cases} \tag{16}$$

This completes the TDPF algorithm in rectangular form capable of estimating the branch temperatures and adjusting the branch resistances. It should be noted that after every iteration, given the calculated branch temperatures, the branch resistances are updated using Equation (1) which is not carried out in the conventional PF. $\frac{\partial g_{ij}}{\partial T_{kn}}$ and $\frac{\partial b_{ij}}{\partial T_{kn}}$ in the above equations can be derived by the chain rule as mentioned in [7].

III. Solar PV Modeling

Consider the PV system coupled to the grid as shown in Fig. 1. The voltage at the PV system output node is $V_{r_{pv}} + jV_{m_{pv}}$, the output current at the node is $I_{r_{pv-grid}} + jI_{m_{pv-grid}}$ which is given by

$$\frac{\partial P_k}{\partial T_{ij}} = \begin{cases} (V_{r_k}^2 - V_{m_k}^2 - V_{r_k}V_{r_j} - V_{m_k}V_{m_j})\dfrac{\partial g_{ij}}{\partial T_{ij}} + (V_{r_k}V_{m_j} - V_{r_j}V_{m_k})\dfrac{\partial b_{ij}}{\partial T_{ij}} & \text{for } i = k \\ (V_{r_k}^2 - V_{m_k}^2 - V_{r_k}V_{r_i} - V_{m_k}V_{m_i})\dfrac{\partial g_{ij}}{\partial T_{ij}} + (V_{r_k}V_{m_i} - V_{r_i}V_{m_k})\dfrac{\partial b_{ij}}{\partial T_{ij}} & \text{for } j = k \\ 0 & \text{for } i, j \neq k \end{cases} \tag{11}$$

$$\frac{\partial Q_k}{\partial T_{ij}} = \begin{cases} (-V_{r_k}^2 - V_{m_k}^2 + V_{r_k}V_{r_j} + V_{m_k}V_{m_j})\dfrac{\partial b_{ij}}{\partial T_{ij}} + (V_{r_k}V_{m_j} - V_{r_j}V_{m_k})\dfrac{\partial g_{ij}}{\partial T_{ij}} & \text{for } i = k \\ (-V_{r_k}^2 - V_{m_k}^2 + V_{r_k}V_{r_i} + V_{m_k}V_{m_i})\dfrac{\partial b_{ij}}{\partial T_{ij}} + (V_{r_k}V_{m_i} - V_{r_i}V_{m_k})\dfrac{\partial g_{ij}}{\partial T_{ij}} & \text{for } j = k \\ 0 & \text{for } i, j \neq k \end{cases} \tag{12}$$

$$\frac{\partial H_{ij}}{\partial T_{kn}} = \begin{cases} 1 - R_\theta(V_{r_i}^2 + V_{r_j}^2 + V_{m_i}^2 + V_{m_j}^2 - 2V_{r_i}V_{r_j} - 2V_{m_i}V_{m_j})\dfrac{\partial g_{ij}}{\partial T_{kn}} & \text{for } kn = ij \\ 0 & \text{for } kn \neq ij \end{cases} \tag{13}$$

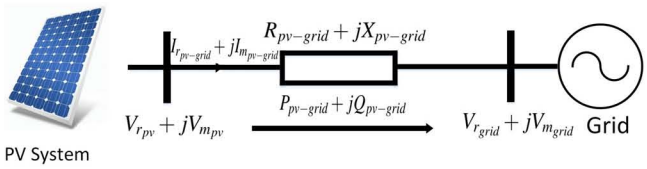

Fig. 1: PV to grid connection.

TABLE I: PV system parameters [4]

Parameter	Value
β_{ref}	0.004 °C^{-1}
T_{ref}	25 °C
T_{NOCT}	46 °C
$T_{\text{a,NOCT}}$	20 °C
G_{NOCT}	800 W/m^2
η_{ref}	0.8

$$I_{r_{pv-grid}} + jI_{m_{pv-grid}} = \frac{(V_{r_{pv}} + jV_{m_{pv}}) - (V_{r_{grid}} + jV_{m_{grid}})}{R_{pv-grid} + jX_{pv-grid}} \tag{17}$$

The power injected to the grid is given by:

$$P_{pv-grid} + jQ_{pv-grid} = (V_{r_{pv}} + jV_{m_{pv}})(I_{r_{pv-grid}} + jI_{m_{pv-grid}})^* \tag{18}$$

The power output of a PV system at unity power factor is given by [13]

$$P_{\text{inverter}} = P_{\text{DC}}\eta_{\text{a}} \tag{19}$$

where $P_{\text{DC}} = P_{\text{input}}\eta_{\text{mp}}$. P_{DC} is the DC power generated by the PV cells due to the solar energy input, P_{input}. The generated DC power depends on various parameters such as: ambient temperature, wind speed, PV cell temperature, Plane of Array (POA) irradiance, etc. [13]. η_{mp} and η_{a} are the maximum power-point efficiency and the efficiency of additional components of the PV system, respectively. η_{mp} is temperature dependent [14] and is given by

$$\eta_{\text{mp}} = \eta_{\text{ref}}\left\{1 - \beta_{\text{ref}}\left[T_{\text{a}} - T_{\text{ref}} + (T_{\text{NOCT}} - T_{\text{a,NOCT}})\frac{G_{\text{T}}}{G_{\text{NOCT}}}\right]\right\} \tag{20}$$

In Equation (20), η_{ref} is the conversion efficiency at standard test conditions, T_{a} is the ambient temperature, T_{ref} is the cell temperature at standard test condition, T_{NOCT} is the nominal operating cell temperature, $T_{\text{a,NOCT}}$ is ambient temperature under the nominal terrestrial environment, G_{T} is the incident radiation on the solar panel, and G_{NOCT} is the global solar flux under nominal terrestrial environment [13]. The PV system injection efficiency has been normalized by dividing P_{DC} with η_{ref} for this study. The PV system parameters used in the study are presented in Table I. The PV systems are considered to be injecting power at unity power factor and are modelled as PQ type [5] nodes for the power flow. This causes the power mismatch $\boldsymbol{\Delta P}$ to become $\boldsymbol{\Delta P = (P_G + P_{pv} - P_L) - P_{calc}}$ for all buses with PV integration. $\boldsymbol{P_G}$ is the power generation into the buses, $\boldsymbol{P_{pv}}$ is the power generation by the PV systems into the buses, $\boldsymbol{P_L}$ is the power consumed by the loads in the buses, and $\boldsymbol{P_{calc}}$ is the net calculated power injection. For the purpose of the study, real solar irradiance data from New Zealand's National Institute of Water and Atmospheric Research's (NIWA) SolarView [15] service was collected. SolarView provides Plane of Array (POA) irradiance data for any location in New Zealand. Fig. 2 presents a day chosen at random from each the four seasons in NZ in 2015. The summer day irradiance curve produces the minimum energy and has the maximum fluctuations most likely due to cloud shading. This summer curve is thus selected for the study to understand the impact of varying solar generation on the network parameters using TDPF. The TDPF also

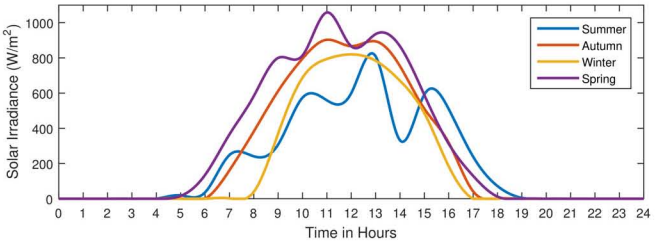

Fig. 2: Typical hourly solar irradiance of a random day in Hawkes Bay for each season in NZ in 2015.

requires knowledge of the ambient temperature, temperature data for the corresponding summer day has been collected from NIWA's national climate database [16] presented in Fig. 3.

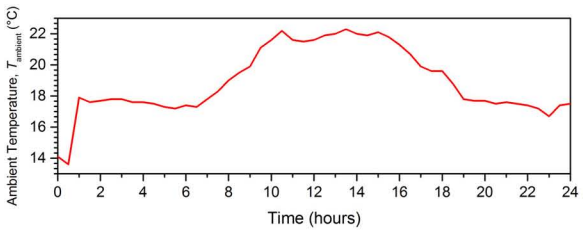

Fig. 3: Ambient temperature throughout the summer day.

IV. IEEE 14-Bus Test Network

The modified single line diagram for the IEEE 14-bus [17] system is shown in Fig. 4. The modification here refers to the addition of PV systems at the load buses. The IEEE 14-bus does not have any conductor specific data, and therefore all conductors were considered to be 795 kcmil 26/7 Drake ACSR conductor reported in IEEE Std. 738 [18]. Using the specifications data for the conductor, selecting a voltage base of 115kV and a complex power base of 100MVA, the lengths of all the overhead conductors were calculated. The network load was slightly modified to enhance the comparison between TDPF and conventional power flow. The network data can be referred to in [17].

V. Simulation Results

For the simulation, a standard desktop computer was used and the algorithms were coded in MATLAB. Bus 1 is the the slack bus and for Bus 2, voltage control was implemented. The rest of the buses were considered as PQ (load) nodes. The PV systems were deployed at a 30% penetration level [19] at all the PQ nodes. As mentioned in the previous section, the summer day solar irradiance curve (Fig. 2) was utilised. Simulations were carried out for every 30mins in the 24-hour day. It is assumed that the conventional PF branch resistances are given at 20°C. The system was initialised with a flat start i.e. all real voltages, V_r, were initialised with 1, all imaginary voltages, V_m, were initialised with 0, and all branch temperatures were initialised with the ambient temperature, T_{ambient}.

An important observation, required for DTLR, that cannot be directly obtained from the conventional PF is the branch temperature profiles. Fig. 5 presents the branch temperatures throughout the day for the three highest loaded branches obtained using the TDPF algorithm. The branches near the source side have the highest temperatures due to maximum power flow in these branches. Around mid-day, as the PV generation increases, the branch loadings are relieved and thus a reduction in branch temperature is observed although the ambient temperature rises. The dotted line in Fig. 5 shows the ambient temperature, T_{ambient}.

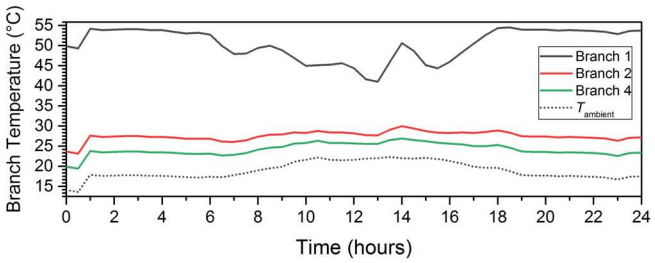

Fig. 5: Temperatures throughout the 24-hour period of the highest loaded branches.

The real power loss (MW) from the conventional PF versus the TDPF and the percentage change in real power loss (MW) compared to the conventional PF are presented in Fig. 6.

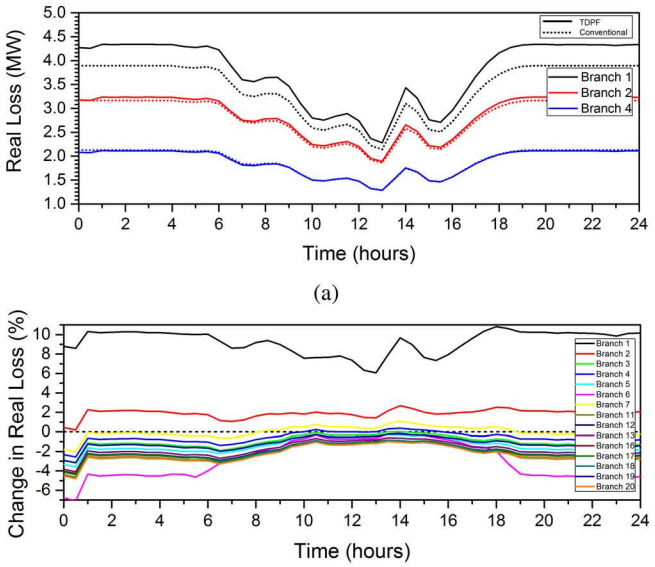

Fig. 6: (a) Real power loss (MW) throughout the day. (b) Percentage change in real power loss of branches throughout the day.

Significant differences in power losses are observed mainly on the source side. The power loss according to the conventional PF in Branch 1 that connects the slack bus to the generator Bus 2 is much lower than the ones calculated from the TDPF indicating that the temperature rise due to the high power loss in highly loaded branches causes significant changes in its resistance. The conventional power loss of Branch 1 is lower by 0.35MW on average compared to the one obtained by TDPF. This under-estimation by the conventional PF could be a significant issue where the power flow is being utilized in electricity pricing, investment planning, network design, etc. [20]. The TDPF helps capture effects which are not accounted for in the conventional PF. The percentage change in branch real loss from the conventional is calculated as

$$\frac{R_{\text{Loss, TDPF}} - R_{\text{Loss, Conventional}}}{R_{\text{Loss, TDPF}}} \times 100\%. \tag{21}$$

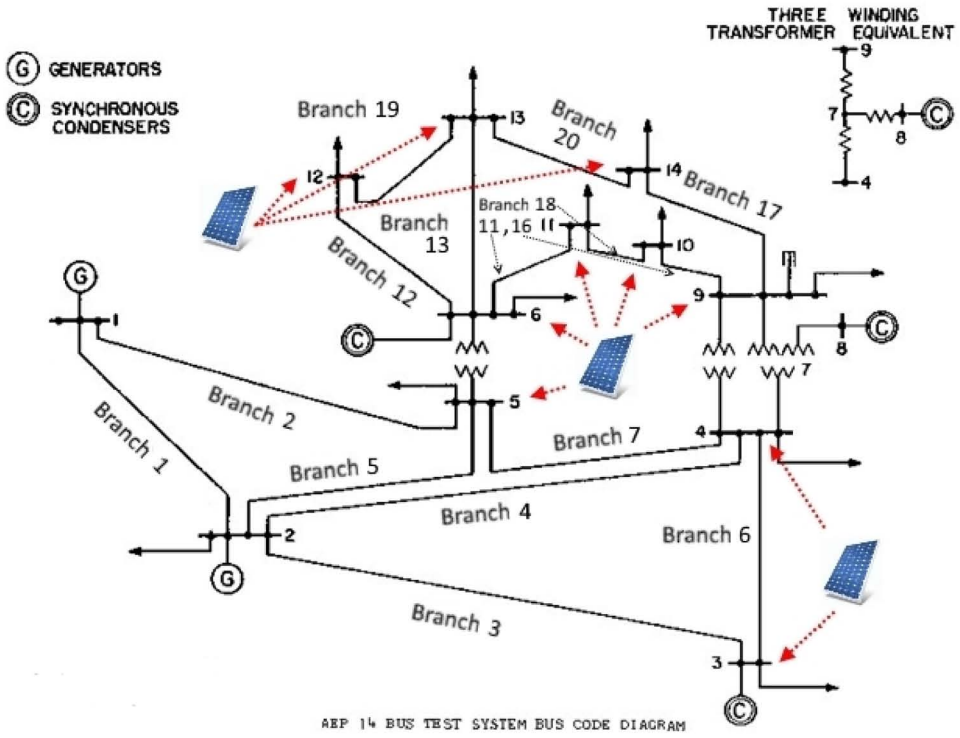

Fig. 4: Modified IEEE 14-Bus test network [17].

A maximum percentage change of +10.8% and a minimum percentage change of -7.1% was observed. The voltage profiles of the buses from conventional PF versus TDPF and the percentage change in the voltage profiles compared to the conventional PF are presented in Fig. 7.

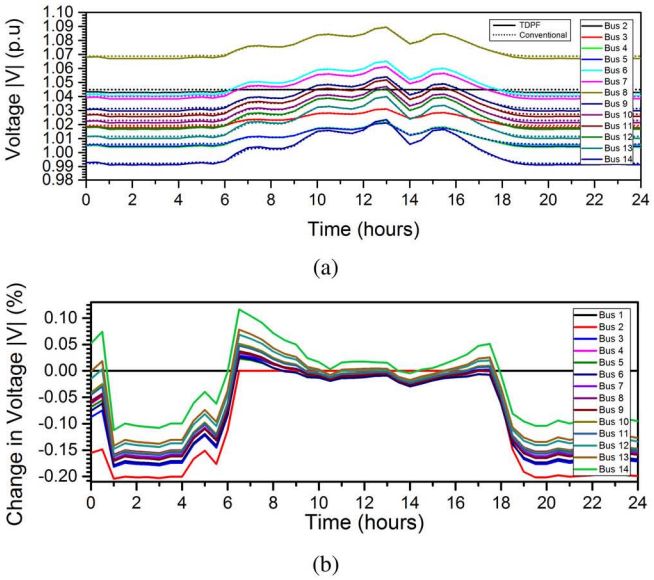

(a)

(b)

Fig. 7: (a) Bus voltage profiles throughout the day. (b) Percentage change in bus voltage profiles throughout the day.

As the ambient temperature increases throughout the day, the bus voltages coincide with conventional PF bus voltages (at 20°C) due to the fact that the data for the conventional PF is assumed for 20°C. Similarly, as the ambient temperature reduces below 20°C after mid-day the differences in voltage magnitudes becomes apparent via the two algorithms. It should be noted that as the generation from the PV increases, Bus 2 still keeps the voltages constant since it is a voltage regulating Bus. The lowest percentage change observed was -0.2% and the highest observed was +0.1%. These changes in voltage profiles observed in a single-day simulation present the importance of TDPF in power system planning, design, and operation [20]. In summary, the results presented show the superiority of the TDPF over the conventional PF algorithm and indicates that it could prove to be an important tool for better power system analyses.

VI. Conclusion

The TDPF is derived and presented in rectangular form in this manuscript. In contrast to the conventional PF, the TDPF algorithm takes into account the conductor temperature-resistance relationship and calculates appropriate resistances every iteration in order to output the PF solution. PV systems were integrated into the algorithms as a PQ node to study the temperature profiles, voltage profiles, and power loss profiles in the network over a single-day simulation. The results show significant changes in calculated power loss and voltage magnitudes compared to a conventional PF, which emphasises

the use of the algorithm to look into time-series power flow analyses for longer time periods. The results indicate the need to use a TDPF in the study of modern smart networks to give more accurate understanding of important power flow related factors. The TDPF also outputs conductor temperatures as a part of the PF solution which can be utilised to conduct DTLR studies to be undertaken in future.

ACKNOWLEDGMENT

The authors acknowledge the support of Victoria University of Wellington for this work through the VUW Research Trust and Robinson Research Institute.

REFERENCES

[1] C. Liu, S. McArthur, and S. Lee, *Smart Grid Handbook*. Wiley, 2016.
[2] M. Bollen, *Integration of Distributed Generation in the Power System*, ser. IEEE Press Series on Power Engineering. John Wiley & Sons, 2011.
[3] O. Elgerd, *Electric Energy Systems Theory*: *An Introduction*. Tata McGraw-Hill, 1983.
[4] J. Widn, E. Wckelgrd, J. Paatero, and P. Lund, "Impacts of distributed photovoltaics on network voltages: Stochastic simulations of three swedish low-voltage distribution grids," *Electric Power Systems Research*, vol. 80, no. 12, pp. 1562 – 1571, 2010.
[5] H. Saadat, *Power System Analysis*. PSA Publishing, 2010.
[6] J. Glover, T. Overbye, and M. Sarma, *Power System Analysis and Design*. Cengage Learning, 2016.
[7] S. Frank, J. Sexauer, and S. Mohagheghi, "Temperature-dependent power flow," *IEEE Transactions on Power Systems*, vol. 28, no. 4, pp. 4007–4018, Nov 2013.
[8] *Aluminium Electrical Conductor Handbook*, 2nd ed. The Aluminium Association, 1982.
[9] J. R. Santos, A. G. Exposito, and F. P. Sanchez, "Assessment of conductor thermal models for grid studies," *IET Generation, Transmission Distribution*, vol. 1, no. 1, pp. 155–161, January 2007.
[10] L. Dawson and A. Knight, "Applicability of dynamic thermal line rating for long lines," *IEEE Transactions on Power Delivery*, vol. PP, no. 99, pp. 1–1, 2017.
[11] S. D. Kim and M. M. Morcos, "An application of dynamic thermal line rating control system to up-rate the ampacity of overhead transmission lines," *IEEE Transactions on Power Delivery*, vol. 28, no. 2, pp. 1231–1232, April 2013.
[12] L. Powell, *Power System Load Flow Analysis*. McGraw-Hill Education, 2004.
[13] J. Duffie and W. Beckman, *Solar Engineering of Thermal Processes*, ser. A Wiley-Interscience Publication. Wiley, 1991.
[14] Q. Kou, S. Klein, and W. Beckman, "A method for estimating the long-term performance of direct-coupled pv pumping systems," *Solar Energy*, vol. 64, no. 1, pp. 33 – 40, 1998.
[15] "Solarview," https://solarview.niwa.co.nz, accessed: 2017-05-30.
[16] "The naitional climate database," https://cliflo.niwa.co.nz, accessed: 2017-05-30.
[17] "14 bus power flow test case, power systems test case archive," http://www2.ee.washington.edu/research/pstca/pf14/pg_tca14bus.htm.
[18] "IEEE standard for calculating the current-temperature relationship of bare overhead conductors," *IEEE Std 738-2012 (Revision of IEEE Std 738-2006 - Incorporates IEEE Std 738-2012 Cor 1-2013)*, pp. 1–72, Dec 2013.
[19] M. Ropp, J. Newmiller, C. Whitaker, and B. Norris, "Review of potential problems and utility concerns arising from high penetration levels of photovoltaics in distribution systems," in *2008 33rd IEEE Photovoltaic Specialists Conference*, May 2008, pp. 1–6.
[20] H. Seifi and M. Sepasian, *Electric Power System Planning: Issues, Algorithms and Solutions*, ser. Power Systems. Springer Berlin Heidelberg, 2011.